Investigation of AlGaN/GaN HEMTs with step aluminum mole fraction and doping level in the barrier layer

Seyed Mohammad Razavi[1*], Seyed Ebrahim Hosseini[**]
[*]Department of Electrical Engineering, University of Neyshabur, Neyshabur, Iran
[**]Faculty of Engineering, Ferdowsi University of Mashhad, Mashhad, Iran
[1]Corresponding Author Email: razavi@neyshabur.ac.ir

Abstract **- Gallium-nitride (GaN) high electron mobility transistors (HEMTs) with step aluminum mole fraction or doping concentration in the barrier is reported. The barrier layer is divided into two Source Side (SS) and Drain Side (DS) parts with the same lengths and thicknesses, but with different aluminum mole fraction or doping levels. Average of the aluminum mole fraction or doping concentration in the barrier is equal to those in the conventional structure. Changes that happen in the maximum lateral electric field, breakdown voltage, maximum DC trans-conductance (g_m), drain current, gate-source capacitance, cut off frequency and DC output conductance (g_o) as a function of different source side (N_{SS}) and drain side (N_{DS}) barrier doping levels or different aluminum mole fractions at source side (X_{SS}) and drain side (X_{DS}) are studied in details. Simulation results illustrate that a smaller N_{DS} compared to N_{SS} improves the breakdown voltage. On the other hand, decreasing N_{SS} reduces the gate-source capacitance and DC output conductance. With varying N_{SS} and N_{DS}, the DC trans-conductance has a nonlinear variation. Also, proposed structures with smaller X_{SS} than X_{DS} reduces the maximum lateral electric field and then improve the breakdown voltage and g_o.**

Keywords- GaN HEMT; Gate-source capacitance; Breakdown voltage; DC output conductance; maximum DC trans-conductance.

I. INTRODUCTION

Gallium nitride high-electron mobility transistors (HEMTs) are great candidates in the field of high-power electronics [1-6]. AlGaN/GaN HEMTs have received much attention for high-power and high frequencies applications because of a high breakdown field in the wide-band gap semiconductors are capable of the high temperature applications [7-8]. In addition to that, a large conduction band discontinuity between GaN and AlGaN and the presence of polarization fields allow a large two-dimensional electron gas (2-DEG) concentration to be confined [9-10]. Improving DC and RF characteristics of these devices is a very important challenge for researchers in this field. In this work, a novel AlGaN/GaN HEMT with step aluminum mole fraction or doping concentration in the barrier is reported. The most important DC and RF parameters of AlGaN/GaN HEMT with different aluminum mole fraction or doping level in the barrier at source and drain sides are explored and compared with those in the conventional [11]. Gate-source capacitance, maximum lateral electric field, breakdown voltage, DC output conductance (g_o), maximum DC trans-conductance (g_m), cut off frequency (f_T) and drain current of the proposed structures are simulated using atlas simulator software. In the next section, the proposed structure dimensions and the physical models used in the 2-D simulations are described in details. In the third section, we first explain how the barrier layer with step aluminum mole fraction or doping concentration in the HEMT will reduce the maximum lateral electric field in the channel and consequently improve breakdown voltage significantly. Also, in this section, the effect of step mole fraction or doping level in the barrier on the drain current, gate-source capacitance, maximum DC trans-conductance, cut off frequency and output conductance of the proposed structure are studied and compared with those in the conventional in details.

II. DEVICE STRUCTURES

Schematic cross-sections of the proposed and conventional [11] structures are shown in Figures 1(a) and (b), respectively. The dimensions of the structures are as follows: gate length L_g=0.5μm, gate-drain spacing L_{gd}=1μm, gate-source spacing L_{gs}=1μm. Barrier layer and channel thicknesses are T_B=22nm and T_C=1.5μm, respectively. The barrier layer in the conventional structure is n-type heavily doped $Al_{0.32}Ga_{0.68}N$ while in the proposed structures, doping and aluminum mole fraction in this layer are varied in the source and drain sides. The channel layer of conventional and proposed structures is an intrinsic GaN. Nickel is chosen for the gate Schottky contact with a work function of 5.1eV. It is worth noting that the proposed and conventional structures can be fabricated using the same procedure as reported in [11]. The devices are simulated using two dimensional ATLAS soft ware[12]. In order to achieve more realistic results, several models are activated in simulations, including the 'SRH' model for Shockley–Read–Hall recombination, the 'Conmob' model for standard concentration dependent mobility, the 'Fldmob' model for parallel electric field-dependent mobility and the 'Fermi Dirac' model for statistics[13-14].

978-1-5090-5963-8/17/$31.00 ©2017 IEEE

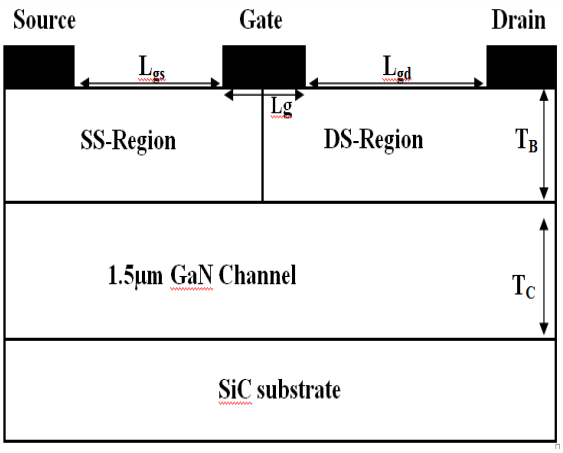

Fig. 1(a)

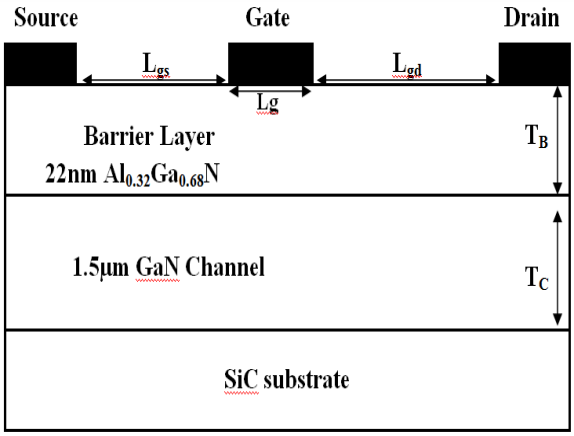

Fig. 1(b)

Fig. 1. Cross sections of the (a) proposed and (b) conventional structures.

III. Results And Discussions

A. Electric Field

Lateral electric field in the channel at V_{DS}=80V and V_{GS}=-4V for different N_{SS} and N_{DS} at a fixed value of X_{SS} and X_{DS} (0.32) is shown in figure 2(a). The electric field curve with N_{SS}=N_{DS}=1×10^{18}cm^{-3} corresponds to the conventional structure. To get a meaningful comparison between the proposed and conventional structures, average of N_{SS} and N_{DS} in the proposed structures is equal to that in the conventional (1×10^{18}cm^{-3}). It is clear from this figure that decreasing N_{DS} in the proposed structures reduces the maximum lateral electric field at the gate corner near the drain compared to the conventional structure. A further investigation shows that the breakdown happened at gate corner near the drain due to the electric field crowding [15-16]. Hence, it can be deduced that the structure with smaller N_{DS} compared to N_{SS} has a larger breakdown voltage than that in the conventional structure. Critical electric field of the GaN (3.5MV/cm) is used to clarify the breakdown voltage [17]. Increasing the drain-source voltage increases the maximum electric field in the channel. The breakdown voltage is nominated the drain-source voltage that the maximum electric field in the channel is equal to the critical electric field. It is obvious from the figure 2(a) that the peak electric field in the channel of the structure with N_{SS}=1.5×10^{18}cm^{-3} and N_{DS}=0.5×10^{18}cm^{-3} is the least peak electric field in the all structures. So, it can be concluded that this structure can be applied at higher drain-source voltage to get to the critical electric field compared to the other structures. Therefore, this structure has the largest breakdown voltage in the investigated structures. The peak electric field of the proposed structures at V_{DS}=80V is lesser than the critical electric field. Thus, the breakdown voltages of the proposed structures are bigger than 80V. As a result from the simulations, in the structure with N_{SS}=1.5×10^{18}cm^{-3} and N_{DS}=0.5×10^{18}cm^{-3}, increasing drain-source voltage up to 220V can move up the maximum electric field in the channel to the critical electric field. This voltage (220V) can be listed as the breakdown voltage in this structure. With applying a similar process, the breakdown voltage of the conventional structure is about 90V. As a result, it can be seen that this proposed structure increases the breakdown voltage significantly. The maximum electric field of the structures with bigger N_{DS} compared to the N_{SS} is larger than that in the conventional structure. So, these structures have smaller breakdown voltage than that in the conventional structure. It is worth noting that smaller N_{DS} compared to N_{SS} can be applied to improve the breakdown voltage in the proposed structures. According to the figure 2(b), the structure with X_{SS}=0.22 and X_{DS}=0.42 has the minimum peak electric field in the channel. For this reason, this structure has the maximum breakdown voltage between the structures with different X_{SS} and X_{DS}. However, it is understandable that in these structures, N_{SS} and N_{DS} have the same value (1×10^{18}cm^{-3}). It is obvious from this figure that in the structures with smaller X_{SS} compared to the X_{DS}, the maximum electric field in the channel is lesser than that in the conventional structure. Consequently, it can be deduced that these structures have bigger breakdown voltage than that in the conventional. Also, the peak electric field in the structures with X_{SS} larger than X_{DS} is equal to that in the conventional structure. So, these structures have the same breakdown voltage with the conventional structure.

B. Drain Current

Drain currents as a function of drain-source voltages for different N_{SS} and N_{DS} are simulated and compared to those in the conventional structure at V_{GS}=0V in fig. 3(a). As illustrated in this figure, the proposed structures decrease the drain current slightly. Decreased drain currents result from the lower 2-DEG density in the channel due to reduction of the barrier layer density in the source or drain side [11]. However, it is worth noting that the proposed structure with N_{SS}=1.25×10^{18} cm^{-3} and N_{DS}=0.75×10^{18}cm^{-3} has bigger saturated drain current than that in the conventional. In linear region, the drain current of the conventional structure is higher than those in the proposed structures. Hence, the best behavior in the saturated drain current is happened in the discussed

978-1-5090-5963-8/17/$31.00 ©2017 IEEE

proposed structure. Figure 3(b) demonstrates the drain current versus drain-source voltage for different X_{SS} and X_{DS} at V_{GS}=0V in the proposed and conventional structures. The drain current in the proposed structure with X_{SS}=0.37 and X_{DS}=0.27 is equal to that in the conventional structures. So, the maximum drain current is obtained in the proposed structure with X_{SS}=0.37 and X_{DS}=0.27 and conventional. As is evident from this figure, in the proposed structures with lesser X_{SS} than X_{DS}, the drain current is reduced significantly. This is due to small X_{SS} in the source side of the proposed structures that reduces the 2-DEG density in this side and then reduces the drain current. The minimum drain current is achieved in the structure with X_{SS}=0.22 and X_{DS}=0.42. It is because this structure has the least value of X_{SS} in the proposed structures.

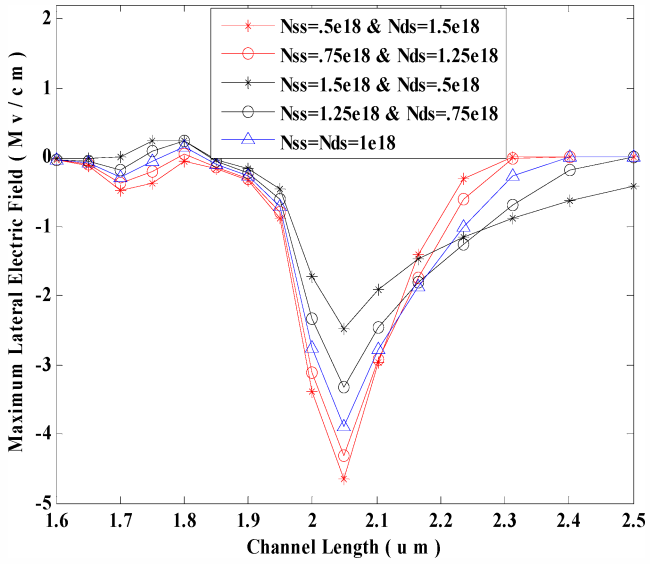

Fig. 2(a)

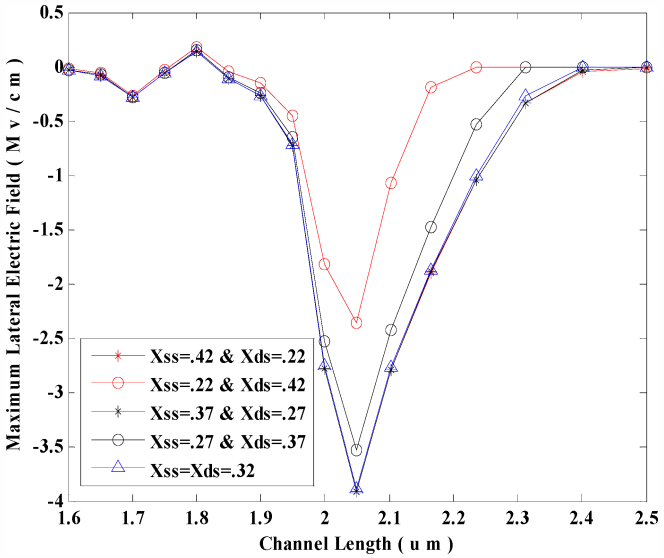

Fig. 2(b)

Fig. 2. Maximum lateral electric field as a function of channel length for (a) different N_{SS} and N_{DS} at a fixed X_{SS} and X_{DS} (0.32) and (b) different X_{SS} and X_{DS} at a fixed N_{SS} and N_{DS} (1×10^{18}cm^{-3}) in the proposed and conventional structures at V_{GS}=-4V and V_{DS}=80V.

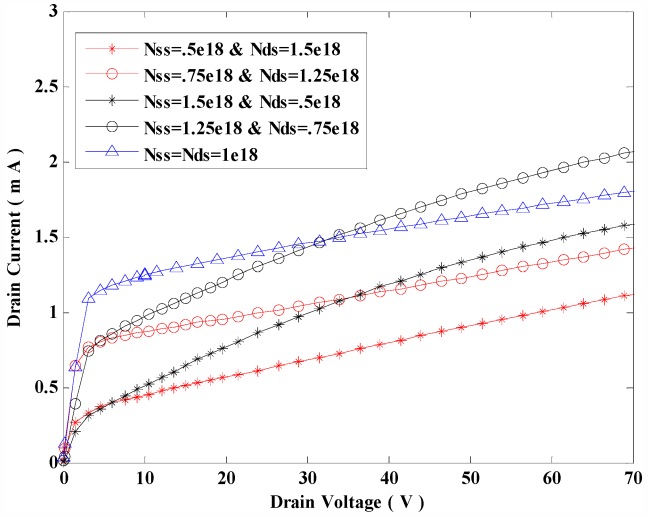

Fig. 3(a)

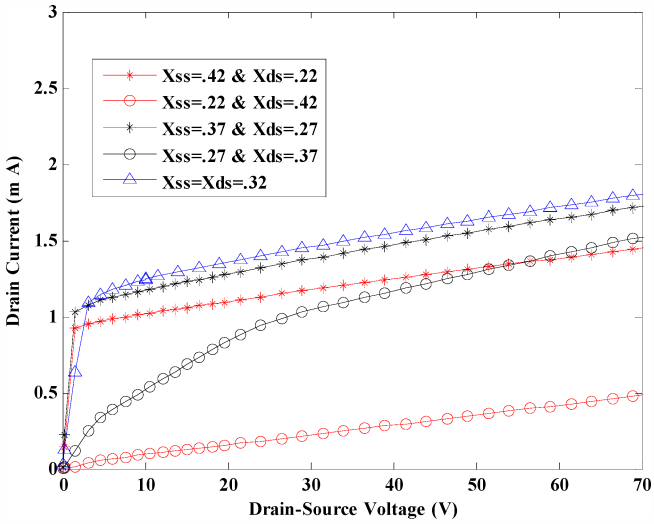

Fig. 3(b)

Fig. 3. Drain currents with respect to drain voltages for (a) different N_{SS} and N_{DS} at a fixed X_{SS} and X_{DS} (0.32) and (b) different X_{SS} and X_{DS} at a fixed N_{SS} and N_{DS} (1×10^{18}cm^{-3}) in the proposed and conventional structures at V_{GS}=0V.

C. *Gate-Source Capacitance*

Figure 4(a) shows the simulated gate-source capacitances (C_{gs}) as a function of the frequency for different N_{SS} and N_{DS} at a similar value of X_{SS} and X_{DS} (0.32) at V_{GS}=0V and V_{DS}=20V conditions. The gate-source capacitance in the structure with N_{SS}=N_{DS}=1×10^{18}cm^{-3} corresponds to the conventional structure. The average of N_{SS} and N_{DS} for different conditions is equal to those in the conventional (1×10^{18}cm^{-3}). According to this figure, a smaller N_{SS} compared to the N_{DS} can be used to decrease the C_{gs}. Smaller value of N_{SS} decreases net electrons density in the channel at

978-1-5090-5963-8/17/$31.00 ©2017 IEEE

the source side, because the net donor impurities density in the barrier at that side is reduced. This in turn decreases the gate-source capacitance and consequently improves high frequency performance [17]. As is displayed in this figure, the minimum gate-source capacitance is obtained for the structure with $N_{SS}=0.5\times10^{18}cm^{-3}$ and $N_{DS}=1.5\times10^{18}cm^{-3}$. Gate-source capacitances with respect to the frequency for different X_{SS} and X_{DS} at a constant N_{SS} and N_{DS} ($1\times10^{18}cm^{-3}$) are illustrated in the figure 4(b). The average of the X_{SS} and X_{DS} is 0.32. As is evident from this figure, for structures with X_{SS} larger than X_{DS}, the gate-source capacitance has lesser value than that in structures with X_{SS} lesser than X_{DS}. Hence, larger X_{SS} in comparison with X_{DS} can be chosen to reduce the gate-source capacitance. The minimum gate-source capacitance is achieved for the structure with $X_{SS}=0.42$ and $X_{DS}=0.22$. As be shown in figures 4(a) and (b), it can be concluded that the structure with smaller N_{SS} compared to N_{DS} and larger X_{SS} compared to X_{DS} can be used to reduce the gate-source capacitance.

D. DC Trans-Conductance

The trans-conductance (g_m) of devices can be calculated by differentiating the drain-source current with respect to gate-source voltage at a constant drain-source voltage [18]:

$$g_m = \left.\frac{\partial I_D}{\partial V_{GS}}\right|_{Vds=const} \quad (1)$$

G_m shows the drain current dependence to gate-source voltage at a fixed drain-source voltage. Figure 5(a) provides a comparison between g_m for different N_{SS} and N_{DS} in the proposed and conventional structures at $V_{DS}=10V$. The displayed g_m curve in the structure with $N_{SS}=N_{DS}=1\times10^{18}cm^{-3}$ corresponds to the conventional structure. This figure reveals that maximum g_m of the proposed structure with $N_{SS}=0.75\times10^{18}cm^{-3}$ and $N_{DS}=1.25\times10^{18}cm^{-3}$ is larger than those in the other proposed structures while the maximum g_m in this structure is equal to that in the conventional structure. As a result from this figure, it is obvious that a larger difference between N_{SS} and N_{DS} causes a significant reduction in the maximum g_m. Small difference between N_{SS} and N_{DS} increases the maximum g_m. Comparison between maximum g_m for different X_{SS} and X_{DS} at $V_{DS}=10V$ is exposed in the figure 5(b). As is discussed in the previous sections, the average of X_{SS} and X_{DS} is similar to that in the conventional (0.32). It is apparent from this figure that the structure with $X_{SS}=0.37$ and $X_{DS}=0.27$ and conventional have the maximum g_m. The structure with the minimum X_{SS} has the minimum g_m. Also, it can be deduced that the structures with smaller X_{SS} than X_{DS} have the lesser maximum g_m than the structures with larger X_{SS} than X_{DS}. Therefore, a larger X_{SS} compared to the X_{DS} in the proposed structures can be used to improve the maximum g_m.

E. Cut Off Frequency

The cut-off frequency (f_T) can be calculated from equation (2) where g_m is the maximum DC trans-conductance and c_{gs} is the gate-source capacitance [19].

$$f_T = \frac{g_m}{2\pi C_{gs}} \quad (2)$$

Equation (2) shows that a larger g_m/C_{gs} ratio improves the f_T. It can be seen from the figs. 4 and 5 that the structure with $N_{SS}=0.75\times10^{18}cm^{-3}$ and $N_{DS}=1.25\times10^{18}cm^{-3}$ at a fixed X_{SS} and X_{DS} (0.32) has larger g_m and smaller C_{gs} than that in the conventional structure. Therefore, this proposed structure has larger g_m/C_{gs} ratio and consequently larger f_T compared to the conventional structure. Also, it is obvious from these figures that the structure with $X_{SS}=0.42$ and $X_{DS}=0.22$ has equal g_m and smaller C_{gs} compared to the conventional structure. Hence, this structure improves f_T in comparison with that in the conventional structure.

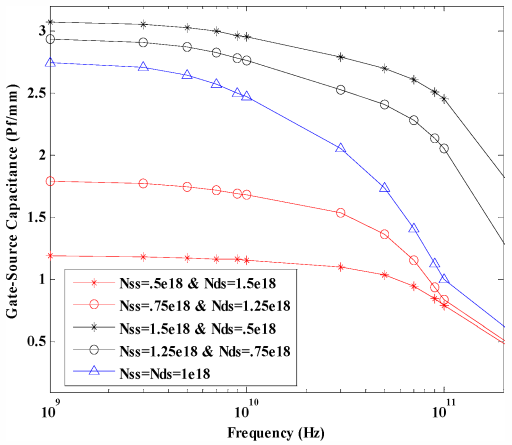

Fig. 4(a)

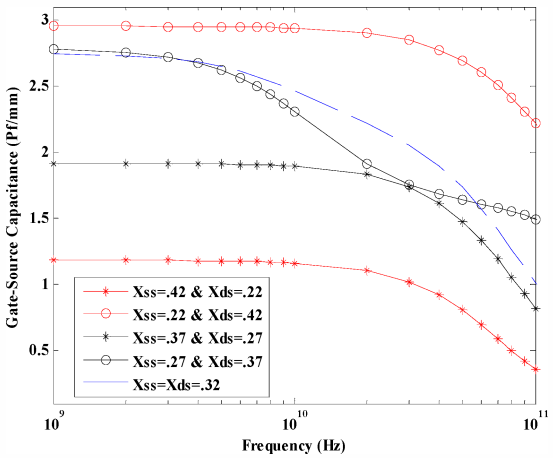

Fig. 4(b)

Fig. 4. Gate-source capacitances as a function of the frequency for (a) different N_{SS} and N_{DS} at a fixed X_{SS} and X_{DS} (0.32) and (b) different X_{SS} and X_{DS} at a fixed N_{SS} and N_{DS} ($1\times10^{18}cm^{-3}$) in the proposed and conventional structures at $V_{GS}=0V$ and $V_{DS}=20V$.

978-1-5090-5963-8/17/$31.00 ©2017 IEEE

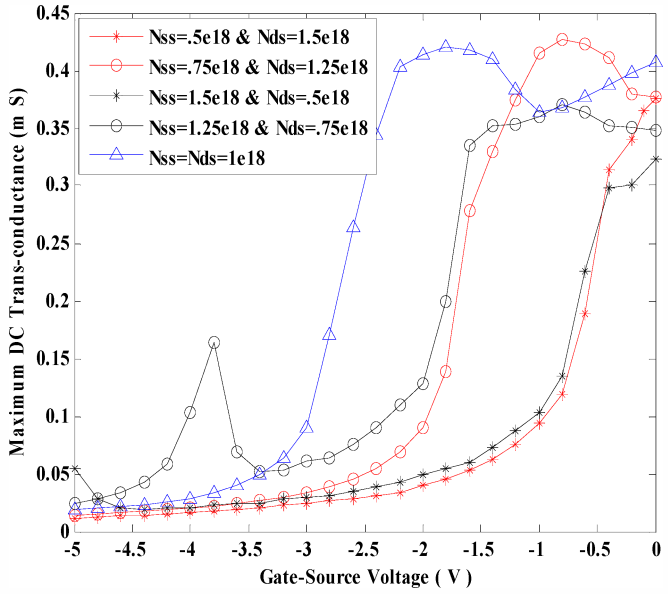

Fig. 5(a)

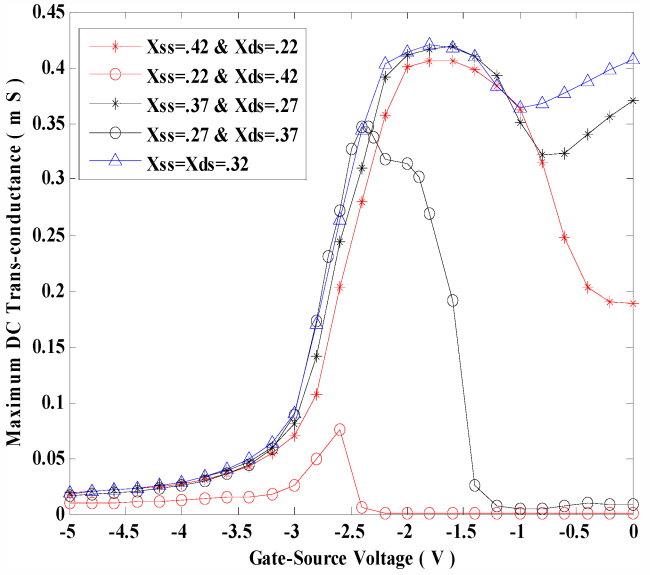

Fig. 5(b)

Fig. 5. Maximum DC Trans-conductance dependence to gate-source voltage for (a) different N_{SS} and N_{DS} at a fixed X_{SS} and X_{DS} (0.32) and (b) different X_{SS} and X_{DS} at a fixed N_{SS} and N_{DS} ($1\times10^{18}cm^{-3}$) in the proposed and conventional structures at V_{DS}=10V.

F. Output Conductance

The output conductance (g_o) of the devices can be calculated by differentiating the drain-source current with respect to drain-source voltage when gate-source voltage is constant.

$$g_o = \frac{\partial I_D}{\partial V_{DS}}\Big\|_{V_{GS}=const} \quad (3)$$

It can be concluded from the equation (3) that g_o shows the drain current dependence to the drain-source voltage for a fixed gate-source voltage. Figure 6(a) shows the output conductance dependence to the N_{SS} and N_{DS} at V_{GS} =-4V in the proposed and conventional structures. In the conventional structure, N_{SS} is equal to the N_{DS}. As is disclosed in this figure, the output conductance of the structures with smaller N_{SS} than N_{DS} is lesser than that in the conventional structure. This is because, as reported in figure 3(a), the drain current versus drain voltage reduces in comparison with the conventional and consequently reduces the output conductance. Also, it can be concluded that in this condition the drain voltage control on the channel is reduced. As is exhibited in this figure, the g_o in the structures with higher N_{SS} compared to N_{DS} is larger than that in the conventional. So, the drain-source voltage control on the channel is increased in these structures. The minimum g_o is obtained at the proposed structure with $N_{SS}=0.5\times10^{18}cm^{-3}$ and $N_{DS}=1.5\times10^{18}cm^{-3}$. With increasing drain voltage for different structures, the output conductance is reduced because the drain current is coming near to the saturation region and then slope of the drain current curve is reduced. The g_o dependence to the drain-source voltage for different X_{SS} and X_{DS} at a fixed N_{SS} and N_{DS} value ($1\times10^{18}cm^{-3}$) is plotted and compared to that in the conventional in the figure 6(b). According to this figure, the proposed structures with smaller X_{SS} than X_{DS} have lesser g_o than that in the conventional. The smallest go in the investigated structures is obtained for the structure with X_{SS}=0.22 and X_{DS}=0.42. In the structures with bigger X_{SS} than X_{DS}, the g_o is equal to that in the conventional structure. Therefore, it can be concluded that smaller X_{SS} compared to X_{DS} can be applied to reduce the g_o.

IV. Conclusion

Important DC and RF parameters of the AlGaN/GaN HEMTs with step doping concentration or aluminum mole fraction in the barrier are reported in details. The gate-source capacitance, maximum g_m, cut off frequency, lateral electric field, breakdown voltage, g_o and drain current in the proposed structures are studied and compared to those of the conventional structure. Our simulation results disclose that the proposed structures improve the breakdown voltage, gate-source capacitance, cut off frequency and g_o in comparison with those in the conventional structure. The maximum drain current and g_m in the proposed structure is equal to those in the conventional. Also, it is clear that the maximum breakdown voltage of the proposed structures (~220V) is significantly larger than that in the conventional (~90V).

978-1-5090-5963-8/17/$31.00 ©2017 IEEE

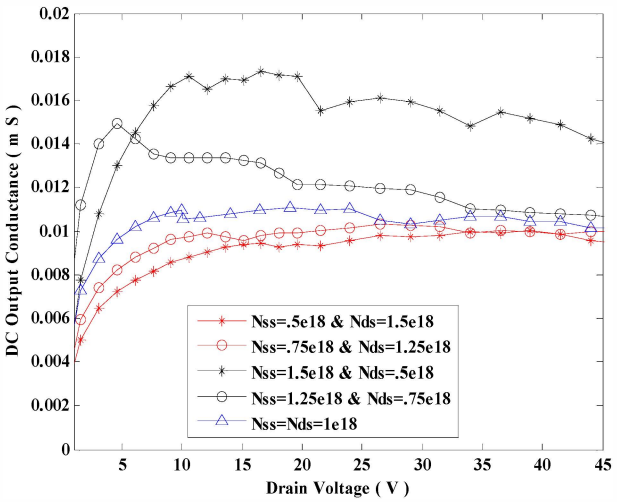

Fig. 6(a)

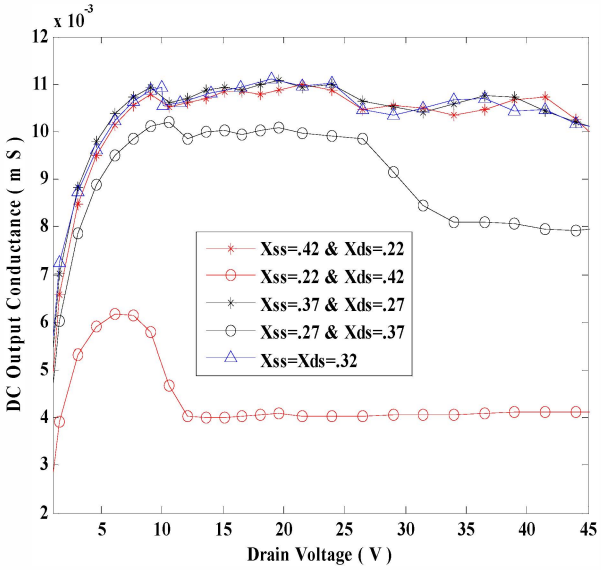

Fig. 6(b)

Fig. 6. Output conductance as a function of drain-source voltage for (a) different N_{SS} and N_{DS} at a fixed X_{SS} and X_{DS} (0.32) and (b) different X_{SS} and X_{DS} at a fixed N_{SS} and N_{DS} ($1\times10^{18}cm^{-3}$) in the proposed and conventional structures at V_{GS} = -4V.

REFERENCES

[1] Y. Ando, Y. Okamoto, H. Miyamoto, T. Nakayama, T. Inoue, and M. Kuzuhara, "10 W/mm AlGaN-GaNHFET with a field modulating plate," *IEEE Electron Device Lett.*, vol. 24, no. 5, pp. 289–291, May 2003.

[2] Y. F. Wu, M. Moore, A. Saxler, T. Wisleder, and P. Parikh, "40 W/mm double field plated GaN HEMTs," in *Proc. Dig. Device Res. Conf.*, Jun. 2006, pp. 151–152.

[3] W. Chong, H. Yunlong, Z. Xuefeng, H. Yue, M. Xiaohua, and Z. Jincheng, "AlGaN/GaNHEMTswith 0.2 µm V-gate recesses for X-band application," *Journal of Semiconductors*, Vol. 33, No. 3, pp. 34003-34006, 2012.

[4] J. Liu, Y. Zhou, J. Zhu, Y. Cai, K.M. Lau, and K. J. Chen, "DC and RF Characteristics of AlGaN/GaN/InGaN/GaN Double-Heterojunction HEMTs," *IEEE Trans. Electron Devices*, Vol. 54, No. 1, pp. 2-10, 2007.

[5] Y. F. Wu, A. Saxler, M. Moore, R. P. Smith, S. Sheppard, P. M. Chavarkar, T. Wisleder, U. K. Mishra, and P. Parikh, "30-W/mm GaN HEMTs by field plate optimization," *IEEE Electron Device Lett.*, vol. 25, no. 3, pp. 117–119, Mar. 2004.

[6] Y. Pei, R. M. Chu, N. A. Fichtenbaum, Z. Chen, D. Brown, L. Shen, S. Keller, S. P. DenBaars, and U. K. Mishra, "Recessed slant gate AlGaN/GaN high electron mobility transistors with 20.9 W/mm at 10 GHz," *Jpn. J. Appl. Phys. 2, Lett.*, vol. 46, no. 45, pp. L1087–L1089, Nov. 2007.

[7] I. Saidi, Y. Cordier, M. Chmielowska, H. Mejri and H. Maaref, "Thermal Effects in AlGaN/GaN/Si High Elec- tron Mobility Transistors," *Solid-State Electronics*, Vol. 61, No. 1, 2011, pp. 1-6.

[8] M. K. Chattopadhyay and S. Tokekar, "Thermal Model for dc Characteristics of Algan/Gan Hemts Including Self-Heating Effect and Non-Linear Polarization," *Micro- electronics Journal*, Vol. 39, No. 10, 2008, pp. 1181-1188.

[9] R. K. Tyagi, A. Ahlawat, M. Pandey and S. Pandey, "An Analytical Two-Dimensional Model for AlGaN/GaN HEMT with Polarization Effects for High Power Applica- tions," *Microelectronics Journal*, Vol. 38, No. 8-9, 2007, pp. 877-883.

[10] E. J. Miller, "Trap Characterization by Gate-Drain Con- ductance and Capacitance Dispersion Studies of an AlGaN/GaN Heterostructure Field Effect Transistor," *Jour- nal of Applied Physics*, Vol. 87, No. 11, 2000, pp. 8070- 8073.

[11] M. Juncai, Z. Jincheng, X. Junshuai, L. Zhiyu, L. Ziyang, X. Xiaoyong, M. Xiaohua, and H. Yue, "Characteristics of AlGaN/GaN/AlGaN double heterojunction HEMTs with an improved breakdown voltage," *Journal of Semiconductors*, Vol. 33, No. 1, pp. 14002-14006, 2012.

[12] ATLAS user's manual: Device simulation software, Silvaco International, September 2005.

[13] **S.E.J. Mahabadi, A.A. Orouji, P. Keshavarzi, and H.A. Moghadam**, "A new partial SOI-LDMOSFET with a modified buried oxide layer for improving self-heating and breakdown voltage," *Semicond. Sci. Technol.,* Vol. 26, pp. 95005-950016, 2011.

[14] **A.A. Orouji, S.M. Razavi, S.E. Hosseini, and H.A. Moghadam**, "Investigation of the novel attributes in double recessed gate SiC MESFETs at drain side," *Semicond. Sci. Technol.,* Vol. 26, pp. 115001-115005, 2011.

[15] C.L. Zhu, Rusli, C.C. Tin, G.H. Zhang, S.F. Yoon, J. Ahn, "Improved performance of SiC MESFETs using double-recessed structure," *Microelectronic Engineering*, Vol. 83, pp. 92–95, 2006.

[16] J. Zhang , X. Luo, Z. Li, B. Zhang," Improved double-recessed 4H-SiC MESFETs structure with recessed source/drain drift region," *Microelectronic Engineering*, Vol. 84, pp. 2888–2891, 2007.

[17] S.M. Razavi, S.H. Zahiri, S.E. Hosseini, "A novel AlGaN/GaN HEMT with a p-layer in the barrier," *Physica E*, Vol. 54, 2013, pp. 24-29.

[18] M. K. Verma and B. B. Pal, "Analysis of Buried Gate MESFET Under Dark and Illumination," *IEEE Trans. Electron Devices*, Vol. 48, No. 9, pp. 2138-2142, 2001.

[19] J. Yang, J. Spann, R. Anderson, and T. Thornton, "High-Frequency Performance of Subthreshold SOI MESFETs," *IEEE Trans. Electron Devices*, Vol. 25, No. 9, pp. 652-654, 2004.

978-1-5090-5963-8/17/$31.00 ©2017 IEEE